Supplementary Table 1: Performance of AGC on six experimental datasets.

dataset	AGC retaining ratio	model to map FSC resolution	half maps FSC resolution	Q-score of raw map	Q-score of sharpened map
		AGC / the original final stack			
TRPA1	93.74%	4.34Å/4.34Å	4.05Å/3.89Å	0.39/0.41	0.45/0.46
hemagglutinin	94.58%	4.53Å/4.47Å	4.06Å/4.11Å	0.41/0.41	0.34/0.35
LAT1	82.46%	3.88Å/3.88Å	3.38Å/3.36Å	0.51/0.51	0.50/0.50
pfCRT	89.48%	4.03Å/3.88Å	3.87Å/3.68Å	0.45/0.50	0.47/0.51
TSHR-Gs	77.46%	3.70Å/3.65Å	3.23Å/3.12Å	0.46/0.47	0.46/0.46
TRPM8	91.54%	3.49Å/3.49Å	3.15Å/3.04Å	0.56/0.60	0.52/0.53

Supplementary Material I: Theoretical analysis of CryoSieve score and simulation verification.

We showed higher CryoSieve score of a particle image ideally indicates that it is of superior quality, rather than being contaminated by typical cryo-EM damage or artifacts. Under the hypothesis that the noise in particles could be modeled as pure Gaussian noise in cryo-EM, we proved the probability of assigning higher CryoSieve score to particles with superior quality was close to 1, as opposed to typical incorrect particles in cryo-EM.

We consider two populations of image patches: good patches, which agree with our 3D reference and bad patches, which have random phased high-frequency components or have incorrect estimated imaging parameters such as rotation angle, in-plane translation, and CTF. Let b_1, b_2 denote random samples from correct and incorrect particle patches, respectively. The effectiveness of CryoSieve score could be written in the following formulation: there is a high probability that CryoSieve score of b_1 is higher than b_2, i.e.,

$$\mathbf{Pr}[g_1 > g_2] > 1 - \eta \quad \text{for a small constant } \eta$$

where

$$g_i = \|Hb_i\|_2^2 - \|H(b_i - \tilde{A}_i x)\|_2^2 = \|b_i\|_H^2 - \|b_i - \tilde{A}_i x\|_H^2$$

H is the chosen highpass operator, $\tilde{A}_i$ is the estimated imaging operator of b_i, x is the reconstructed density map.

Theorem 1 *Let $b_i = A_i x_i + \varepsilon_i$, where A_i is the true (oracle) imaging operator of particle b_i, x_i is the oracle 3D density of the molecule for particle b_i, and ε_i is the noise. Let g_i be the CryoSieve score of the corresponding particle b_i. If $\varepsilon_i \overset{\text{i.i.d}}{\sim} N(0, \sigma^2 I)$, then*

$$\mathbf{Pr}_{\varepsilon_1,\varepsilon_2}[g_1 > g_2] =$$

$$1 - \operatorname{erf}\left(- \frac{\|A_1x_1 - \tilde{A}_1 x\|_H^2 - \|A_1x_1\|_H^2 - \|A_2x_2 - \tilde{A}_2x\|_H^2 + \|A_2x_2\|_H^2}{2\sigma\sqrt{\|\tilde{A}_1x\|_H^2 + \|\tilde{A}_2x\|_H^2}} \right), \tag{1}$$

where $\tilde{A}_i$ is the estimated imaging operator of particle b_i, $\operatorname{erf}(\cdot)$ is the cumulative distribution function of the standard normal distribution.

Proof It is observed that

$$\begin{aligned} g_i &= \|b_i\|_H^2 - \|b_i - \tilde{A}_i x\|_H^2 \\ &= 2\langle b_i, \tilde{A}_i x\rangle_H - \|\tilde{A}_i x\|_H^2 \\ &= 2\langle A_i x_i + \varepsilon_i, \tilde{A}_i x\rangle_H - \|\tilde{A}_i x\|_H^2 \\ &= 2\langle A_i x_i, \tilde{A}_i x\rangle_H + 2\langle \varepsilon_i, \tilde{A}_i x\rangle_H - \|\tilde{A}_i x\|_H^2 \\ &= \|A_i x_i\|_H^2 + 2\langle \tilde{A}_i x, \varepsilon_i\rangle_H - \|A_i x_i - \tilde{A}_i x\|_H^2 \end{aligned}$$

Hence

$$g_1 - g_2 \sim N(-\|A_1x_1 - \tilde{A}_1x\|_H^2 + \|A_1x_1\|_H^2 + \|A_2x_2 - \tilde{A}_2x\|_H^2 - \|A_2x_2\|_H^2, \\ 4(\|\tilde{A}_1x\|_H^2 + \|\tilde{A}_2x\|_H^2)\sigma^2)$$

Then

$$\mathbf{Pr}[g_1 > g_2] = 1 - \mathrm{erf}(-\frac{\|A_1x_1 - \tilde{A}_1x\|_H^2 - \|A_1x_1\|_H^2 - \|A_2x_2 - \tilde{A}_2x\|_H^2 + \|A_2x_2\|_H^2}{2\sigma\sqrt{\|\tilde{A}_1x\|_H^2 + \|\tilde{A}_2x\|_H^2}})$$

□

There may be many kinds of factors contributing to an incorrect particle. In this study, we focus on two specific types of errors: those resulting from high-frequency components random phased, and those caused by inaccurate estimation of imaging parameters such as rotation angle, in-plane translation, and CTF parameters. The first type of erroneous particles involved randomly damaging high-frequency components in the Fourier domain by introducing random phases, while the second type of erroneous particles is associated with errors in parameter estimation.

For random phase error, we assume that the reconstructed density map and the estimated pose parameters are already precise enough, but the erroneous particle is imaged from a radiation damaged molecule. In particular, we assume in Theorem 1 that $A_i = \tilde{A}_i$, $x_1 = x$ while $x_2 = Rx$ where R is a radiation damaging operator. In cryo-EM, we can model radiation damage by high-frequency band random phasing operator.

Then

$$\mathbf{Pr}[g_1 > g_2] = 1 - \mathrm{erf}(\frac{-\|A_1x\|_H^2 - \|A_2x - A_2Rx\|_H^2 + \|A_2Rx\|_H^2}{2\sigma\sqrt{\|A_1x\|_H^2 + \|A_2x\|_H^2}}) \tag{2}$$

For simplicity, we further assume that the imaging operator is not random, that is, $A_1 = A_2 = A = T \circ C \circ P$. Here P is the projection operator, C is the CTF covolution operator, T is the in-plane translation operator.

Then

$$\begin{aligned}\mathbf{Pr}[g_1 > g_2] &= 1 - \mathrm{erf}(\frac{-\|Ax\|_H^2 - \|A(I-R)x\|_H^2 + \|ARx\|_H^2}{2\sqrt{2}\sigma\|Ax\|_H}) \\ &= 1 - \mathrm{erf}(\frac{-\|TCPx\|_H^2 - \|TCP(I-R)x\|_H^2 + \|TCPRx\|_H^2}{2\sqrt{2}\sigma\|TCPx\|_H}) \\ &= 1 - \mathrm{erf}(\frac{-\|CPx\|_H^2 - \|CP(I-R)x\|_H^2 + \|CPRx\|_H^2}{2\sqrt{2}\sigma\|CPx\|_H}) \\ &= 1 - \mathrm{erf}(\frac{-\|\hat{H}\hat{C}\hat{S}\hat{x}\|^2 - \|\hat{H}\hat{C}\hat{S}(I-\hat{R})\hat{x}\|^2 + \|\hat{H}\hat{C}\hat{S}\hat{R}\hat{x}\|^2}{2\sqrt{2}\sigma\|\hat{H}\hat{C}\hat{S}x\|})\end{aligned}$$

Here $\hat{S}$ is the Fourier transform of P, which denotes the slice operator in Fourier domain according to the central slice theorem. Assume the frequency of random phase is equal to the high-pass frequency, then

$$\begin{aligned}\mathbf{Pr}[g_1 > g_2] &= 1 - \mathrm{erf}(-\frac{\|I-\hat{R}\|^2_{Frob}\|\hat{H}\hat{C}\hat{S}\hat{x}\|}{2\sqrt{2}\sigma}) \\ &= 1 - \mathrm{erf}(-\frac{\|I-\hat{R}\|^2_{Frob}\sqrt{f}\|\hat{C}\hat{S}\hat{x}\|}{2\sqrt{2}\sigma}) \\ &= 1 - \mathrm{erf}(-\frac{\|I-\hat{R}\|^2_{Frob}N\sqrt{f\cdot \mathrm{SNR}}}{2\sqrt{2}})\end{aligned}$$

where $f = \frac{\|\hat{H}\hat{C}\hat{S}\hat{x}\|^2}{\|\hat{C}\hat{S}\hat{x}\|^2}$ is the fraction of high-frequency band energy, $\mathrm{SNR} = \frac{\|\hat{C}\hat{S}\hat{x}\|^2}{N^2\sigma^2}$ is the signal-to-noise ratio, and N is the box size of the particle.

Another type of incorrect particles are those with inaccurate estimation of imaging parameters, such as incorrect rotation angle, in-plane translation and CTF parameters. In particular, we assume that $x_1 = x_2 = x$, $A_1 = \tilde{A}_1$ while $A_2 \neq \tilde{A}_2$ in Theorem 1.

Then

$$\mathbf{Pr}[g_1 > g_2] = 1 - \mathrm{erf}(\frac{-\|A_1x\|^2_H - \|A_2x - \tilde{A}_2x\|^2_H + \|A_2x\|^2_H}{2\sigma\sqrt{\|A_1x\|^2_H + \|\tilde{A}_2x\|^2_H}})$$

For simplicity, we further assume that $A_1 = A_2 = A = T\circ C\circ P$ and $\tilde{A}_2 = \tilde{A}$ is the incorrect estimated image operator which involves three cases: $\tilde{A} = \tilde{T}\circ C\circ P$(transition error), $\tilde{A} = T\circ\tilde{C}\circ P$(CTF error), $\tilde{A} = T\circ C\circ\tilde{P}$(projection angle error).Then we have

$$\mathbf{Pr}[g_1 > g_2] = 1 - \mathrm{erf}\left(-\frac{\|H(A-\tilde{A})x\|^2_2}{2\sigma\sqrt{\|HAx\|^2_2 + \|H\tilde{A}x\|^2_2}}\right) \tag{3}$$

Using the derived probability in Equation 2 and Equation 3, extensive simulations are provided to test the performance of CryoSieve score.

We conducted several numerical experiments to test the validity of CryoSieve score with Equation 2 and Equation 3. Assume that x is the reconstructed density map from all particles of eukaryotic cyclic nucleotide-gated channel (CNG), with the resolution of 3.5Å. Let correct particles be the projection of the reconstructed map followed by the CTF convolution, while the incorrect particles were obtained by disturbing the correct particles in the following ways: random phase high-frequency component, incorrect rotation angle, incorrect translation, and incorrect CTF estimation, respectively. The cutoff frequency of the highpass operator H was set to 15Å. For two typical SNRs, we plotted the probability versus the incorrectness of particles, denoted as the disturb of defocus in CTF, the frequency of high-frequency random phase, the in-plane translation error and the disturb of projection angle, respectively (Supplementary Figure 1). The figure shows that the CryoSieve score achieves high accuracy for typical incorrect particles in cryo-EM, even at extremely low SNR of 0.001.

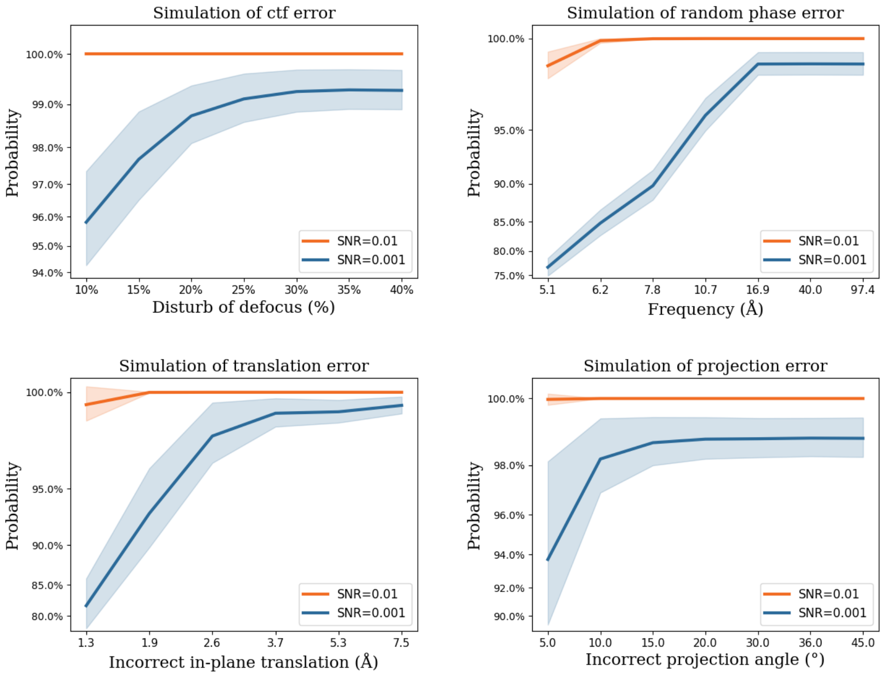

Supplementary Figure 1: **Theoretical probability of correct classification of simulated incorrect particles.** Incorrect particles with random phased high-frequency component, incorrect rotation angle, incorrect in-plane translation and incorrect CTF estimation were generated, respectively. The probability of assigning higher CryoSieve scores to correct particles could be writen as a function of the incorrectness of bad particles. The x-axis represents the degree of incorrectness for simulated bad particles, increasing from left to right. The orange and blue curves depict the mean probability of 10000 independent simulation experiments for different SNRs. Error bars represent the standard deviation of the same simulation experiments, with rotation angle of the correct particles randomly sampled from $SO(3)$ (light orange area, light blue area).

Supplementary Material II: Comparision between CryoSieve and cisTEM

To analyze the properties of the cisTEM score in the six experimental datasets, we split the particles into two subsets, preserving the splitting in the original final stacks. We independently ran *Auto Refine* of cisTEM v1.0.0-beta with default parameters for each half set, resulting in a cisTEM score for each particle image. The particles in each half set were sorted in descending order of the cisTEM score, and particles with higher scores were selected, with the number of selected particles equivalent to that of CryoSieve. Finally, the selected particles were used for 3D density map generation by *ab initio* reconstruction of cryoSPARC, with splits preserved from input alignments by disabling "`Force re-do GS split`". We followed the same procedure and analysis setting as described in the Methods section. CryoSieve outperformed cisTEM in all tested experimental datasets (Supplementary Figure 2).

CryoSieve was compared with cisTEM in the task of removing simulated radiation-damaged particles. As iteration proceeded, the retention rate decreased. CryoSieve achieved higher accuracy than particle selection based on the cisTEM score, especially for particles with relatively low radiation damage (Supplementary Figure 2a). CryoSieve also outperformed cisTEM, as measured by the model-to-map FSC of the reconstructed density map using the retained particles (Supplementary Figure 2b).

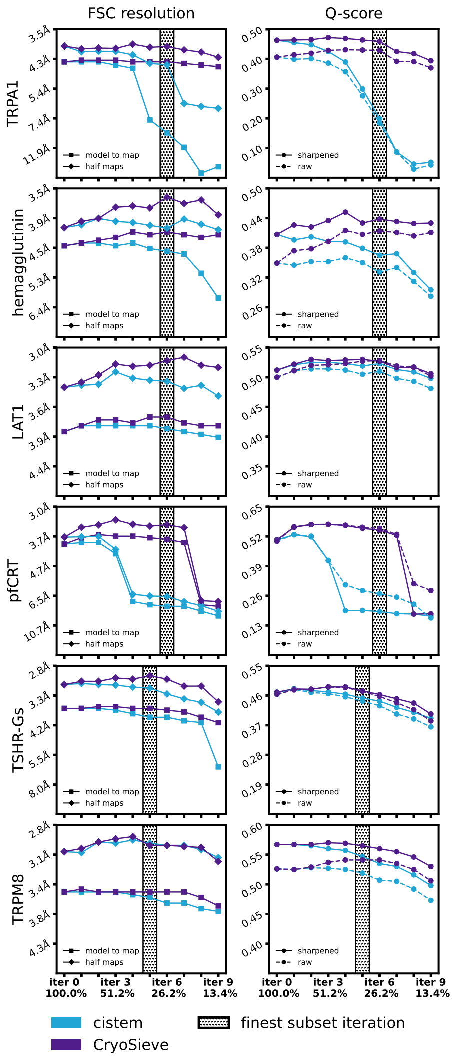

Supplementary Figure 2: **CryoSieve outperformed cisTEM, as measured by FSC-based resolutions and Q-scores.** We compared the density maps reconstructed from retained particles obtained by CryoSieve (indigo) and cisTEM (blue) at different retention ratios. Four metrics were employed for measuring density map quality: FSC-based resolutions, including model-to-map (solid lines with squares) and two-half-maps (solid lines with diamonds) resolutions, are shown in the first column; meanwhile, Q-scores of the raw maps (dashed lines with circles) and the sharpened maps (solid lines with circles) are shown in the second column, as Q-score varies by the B-factor used for sharpening. B-factors for sharpening were self-determined by CryoSPARC. The iterations where CryoSieve obtained the finest subset, determined via comprehending these metrics, are labeled with hatched bars.

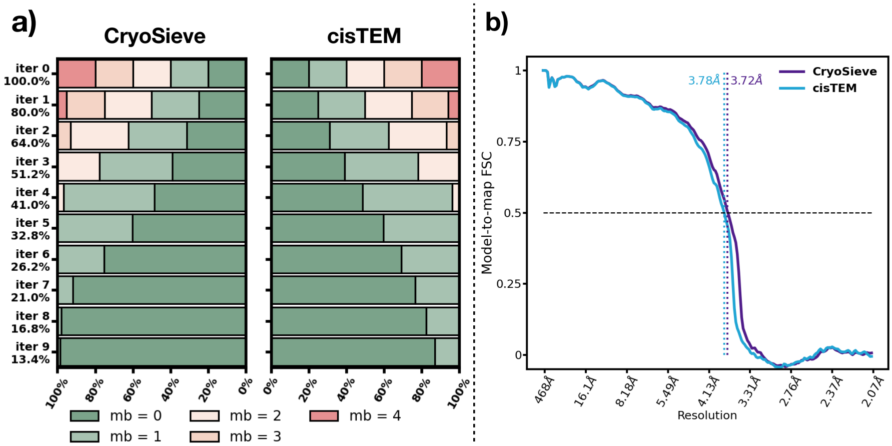

Supplementary Figure 3: **CryoSieve outperformed cisTEM in the removal of radiation-damaged particles. (a)**, At different retention ratios (labelled on the left), the proportions of particles with varying levels of radiation damage (distinguished by colours) in retained particles are shown. The retained particles obtained by CryoSieve (left horizontal bars) and cisTEM (right horizontal bars) were compared. CisTEM performed acceptably for particles with high radiation damage, but still performed inferiorly to CryoSieve for particles with relatively low radiation damage. The accuracy, i.e., the proportion of zero radiation damage particles, of CryoSieve was 91.7% at iteration 7 (rention ratio is 21.0%), while cisTEM's accuracy was only 76.7%. **(b)**, Model-to-map FSCs of the reconstructed density maps using the retained particles were compared. The retention ratio is 21.0% (iteration 7), and retained particles were obtained by CryoSieve (indigo) and cisTEM (blue). The FSC threshold (FSC = 0.5) was depicted as a horizontal dashed line. The FSC of CryoSieve was higher than that of cisTEM, indicating that CryoSieve was more effective in retaining particles with higher resolution information.